Electron, spin-wave, hyperfine, and phonon contributions to the low-temperature specific heat of $La_{0.65}Ca_{0.35}MnO_3$: Effects of magnetic fields and $^{16}O/^{18}O$ exchange

R. A. Fisher, F. Bouquet, and N. E. Phillips
MSD, Lawrence Berkeley National Laboratory and Department of Chemistry, University of California, Berkeley, California 94720

J. P. Franck and Guanwen Zhang
Department of Physics, University of Alberta, Edmonton, Alberta, Canada T6G 2J1

J. E. Gordon
Physics Department, Amherst College, Amherst, Massachusetts 01002

C. Marcenat
Département de Recherche Fondamentale sur la Matière Condensée, Service de Physique, Magnétisme et Supraconductivité, CEA-Grenoble, 38054, Grenoble, France

(Received 1 June 2001; published 13 September 2001)

The field-dependent low-temperature specific heat of an optimally doped polycrystalline sample of $La_{0.65}Ca_{0.35}MnO_3$ ($T_C = 265$ K), $1 \leqslant T \leqslant 32$ K and $0 \leqslant H \leqslant 9$ T was analyzed by a global least-square fit to separate the hyperfine, electronic, spin-wave, and lattice contributions. The hyperfine and spin-wave contributions are in quantitative agreement with nuclear magnetic resonance and inelastic neutron-scattering results, respectively. This agreement supports the validity of both the data and their analysis. The calculated band-structure electron density of states is enhanced by a factor of 1.25. Specific heat was measured for two pieces cut from the ^{16}O parent sample and processed in parallel to produce an ^{18}O and a reference ^{16}O sample. The parallel-processed samples have very much larger lattice contributions ($\sim$50% at low temperatures) than the parent sample, and a somewhat larger electronic contribution. Evidently, the many processing cycles needed for ^{18}O homogeneity produced modifications to both the long-wavelength phonons and the electron density of states. The spin-wave contribution has a small shift—nearly within the experimental accuracy—expected for the $^{18}O/^{16}O$ exchange, while the hyperfine contribution is independent of isotope composition.

DOI: 10.1103/PhysRevB.64.134425 PACS number(s): 65.40.Ba, 75.30.Ds, 75.30.Vn, 75.40.Cx

I. INTRODUCTION

In addition to the unusual transport properties, which suggested the term ''colossal magnetoresistance'' (CMR), certain alkaline-earth-doped rare-earth manganites show an unusual ferromagnetic ordering to a low-temperature, half-metallic state at the Curie temperature (T_C). At high temperatures the properties of these materials, including T_C, depend strongly on oxygen mass. At low temperatures four contributions to the specific heat C associated with the electron density of states (EDOS), ferromagnetic spin waves (FSW), lattice vibrations, and hyperfine interactions can be expected, and some of these may depend on oxygen mass. The number, magnitudes, and the possibility of different magnetic-field H and temperature dependences of these contributions create a problem in the analysis of the experimental data.

There have been prior low-temperature specific-heat measurements on ^{16}O samples of similar composition for Ca,[1–6] Sr,[1,6–8] and Ba (Refs. 1 and 3) substitutions in the $LaMnO_3$ compound. All of the measurements were for $H = 0$, except those of Refs. 6 and 8. An analysis of the low-temperature specific heat showed that all of the data, except for Ref. 6, had a γT term. A $T^{3/2}$ ferromagnetic spin-wave term, to be expected on the basis of neutron-scattering experiments,[9–13] was found for some of the specific-heat data[5–8] but not for others.[1–4]

This paper reports low-temperature specific-heat measurements on a well-characterized, optimally doped CMR material $La_{0.65}Ca_{0.35}MnO_3$ for both ^{16}O and ^{18}O samples. The measurements cover the temperature range $1 \leqslant T \leqslant 32$ K in magnetic fields $0 \leqslant H \leqslant 9$ T. The temperatures and field ranges of the data permit a definitive separation of the four contributions. For $H = 0$ the measurements were extended to 120 K, and in another cryostat from $95 \leqslant T \leqslant 300$ K. They are part of an extensive set of related measurements on the same or similar samples, which include magnetization from 5 to 300 K as a function of H, and near the ferromagnetic metal-insulator transition at $T_C(0) = 265$ K, resistivity as a function of both pressure and H, thermal expansion as a function of H, velocity of sound, and specific heat in magnetic field. The low-temperature specific-heat measurements reported in this paper were made to determine the contributions from the electron density of states, the ferromagnetic spin waves, the Mn hyperfine magnetic field, and the lattice, and to ascertain the effects of magnetic fields and $^{16}O/^{18}O$ exchange on these contributions.

II. EXPERIMENT

The polycrystalline sample of $La_{0.65}Ca_{0.35}MnO_3$ was prepared from high-purity La_2O_3, $CaCO_3$, and MnO_2 powders (all 99.999% pure), which were repeatedly sintered at 1200 °C in air with grinding between each step. A total of

 ©2001 The American Physical Society

eight sintering steps with a total time of 127 h at 1200 °C were done. The calorimetric sample was prepared from this powder by pressing it into a right-circular cylinder and sintering in air (1200 °C, 12 h) followed by sintering in flowing high-purity oxygen (1225 °C, 48 h), and then cooling at 1 °C min^{-1} to room temperature. After the air sintering the sample had 86% of the x-ray density of 5.970 g cm^{-3}, and after the oxygen sintering the density increased to 93%. Samples, similarly prepared by us, were investigated by Heilman *et al.*[14] for the total oxygen content using thermoelectric-power measurements and powder x-ray analysis. They found that there was no observable deviation from a stoichiometric O content of 3.000. This was not only true for ^{16}O samples, but also for the ^{16}O and ^{18}O samples processed in parallel for the isotope-effect experiments. X-ray diffraction was used to check for phase purity and the samples was characterized by measuring the magnetization M as a function of H and T. The sample molecular weight (MW) is 207.25 g mol^{-1} and the theoretical molar volume V is 34.7 cm^3 mol^{-1}.

Sample *A*, 2.27 g, was attached to the calorimeter platform using a small amount of Apiezon *N* Grease (~2 mg) of known heat capacity to ensure good thermal contact. Specific-heat measurements were made for $1 \leqslant T \leqslant 32$ K for $H = 0$, 2, 5, and 9 T using a semiadiabatic heat-pulse method that utilizes a calibrated Cernox thermometer; and from 30 $\leqslant T \leqslant 120$ K and $H = 0$ using a continuous-heating method with a calibrated platinum resistance thermometer. Both sets of measurements had precision and accuracy of about $\pm 0.1\%$ and $\pm 0.5\%$, respectively, for the total measured heat capacity (addenda plus sample). Between 1 and 6 K, the heat capacity of sample *A* varied monotonically from 93 to 60% of the total, and then remained approximately constant at 60% to 12.5 K.

After the specific-heat measurements, sample *A* was cut into two approximately equal pieces (samples *A*1 and *A*2). As a check on the sample homogeneity, specific-heat measurements were made on one of these pieces, sample *A*1, for the temperature range $1 \leqslant T \leqslant 12.5$ K for $H = 0$, 1, 2, 3, 5, 7, and 9 T. Although sample *A*2 was not measured directly, the specific heat was obtained by subtraction of the specific heat of sample *A*1 from that of Sample *A*. The specific heats of samples *A*1 and *A*2 agreed with that of sample *A* to within $\pm 1.5\%$ for ~90% of the points, with the remaining ~10% falling within $\pm 2\%$. Sample *A*'s homogeneity is confirmed by the good agreement among the three data sets. Samples *A*1 and *A*2 were also used for continuous-heating specific-heat measurements near T_C for $H = 0$. In addition, the continuous-heating technique was used to measure the specific heat of sample *A*1 near $T_C(H)$ in magnetic fields to 8 T. The specific-heat data near T_C will be published separately.[15]

Following the above measurements, samples *A*1 and *A*2 were either ^{16}O or ^{18}O exchanged in 1 atm of flowing gas, using an apparatus for simultaneous parallel processing of two samples described previously,[16] to produce samples *A*1*E* and *A*2*E*, respectively. (The "*E*" in the sample labels designates the additional processing and O exchange.) Except for the $^{16}O_2$ or $^{18}O_2$ atmospheres, the two pieces were treated identically, and were processed in parallel under conditions

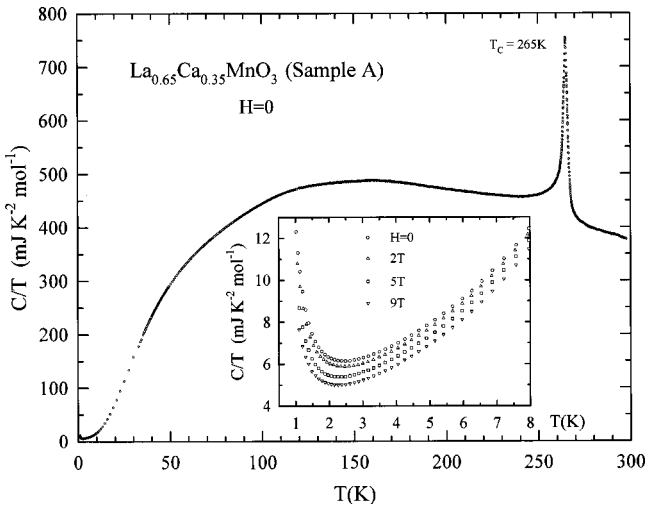

FIG. 1. $C(0)/T$ vs T for $La_{0.65}Ca_{0.35}MnO_3$ (sample A) from 1 to 280 K for $H = 0$. The inset shows the low-temperature specific heat in magnetic fields to 9 T.

similar to that for sample *A*. The specific heat near T_C for Sample *A*1*E* had a double-peaked structure indicating an inhomogeneous ^{18}O distribution. Therefore, both samples were ground and treated several times as powders in 1 atm air at 1050 °C. They were then re-ground and new cylinders pressed. Six additional parallel-processing cycles were necessary to ensure homogeneous ^{18}O distribution, where the annealing temperatures/times were Cycle 1, 1000 °C/48 h; Cycle 2, 1000 °C/96 h; Cycle 3, 1050 °C/48 h; Cycle 4, 1225 °C/48 h; Cycle 5 (regrind, repress, new $^{18}O_2$ supply), 1000 °C/120 h; Cycle 6, 1200 °C/264 h. Magnetization measurements were used to characterize the samples following each cycle. Following Cycle 6, sample *A*1*E* had a density 86.9% of theoretical, and an ^{18}O content $\geqslant 85\%$ with a MW of 212.35 g mol^{-1}. Sample *A*2*E* had a density 81.8% of theoretical. Low-temperature specific-heat measurements were made on both the 0.60-g sample *A*1*E* (^{18}O) and the 0.46-g sample *A*2*E* (^{16}O), each from $1 \leqslant T \leqslant 12.5$ K in magnetic fields of 0, 2, 5, and 9 T. (The specific heat for both samples was increased by a large amount when compared with samples *A*, *A*1, and *A*2, presumably because of the many parallel-processing cycles—see below in Sec. III B for details.)

III. RESULTS AND ANALYSIS

A. Original ^{16}O samples

Figure 1 shows the specific heat for $H = 0$ over the entire range of temperature, 1–300 K, plotted as C/T vs T. The low-T specific heats of sample *A* are shown in the inset for different *H*. A common impurity phase in the manganites is the spinel Mn_3O_4.[17] It orders ferromagnetically near 43 K with a prominent double-peaked structure in C/T (Ref. 18) that is observable in some manganite samples[17] even for relatively small quantities. The present data show no trace of such structure. There is a large sharp anomaly in C/T associated with the ferromagnetic ordering of the Mn with $T_C = 265$ K. When a smooth curve is interpolated through the

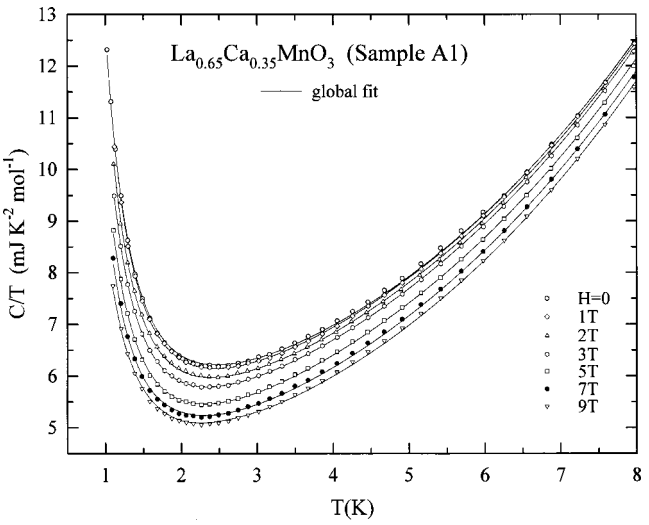

FIG. 2. $C(H)/T$ vs T below 8 K for $La_{0.65}Ca_{0.35}MnO_3$ (sample A1). The curves through the data are from a global least-square fit with an H-dependent γ.

region of this anomaly, from well above and below T_C, the entropy between this curve and the anomaly is only ~16% of that expected for the Mn ordering. It is very improbable that the entropy associated with the EDOS and spin-wave contributions below T_C can account for all of the ~84% remaining entropy—see below in Sec. IV. Therefore, a relatively large amount of entropy must be removed above T_C by, e.g., polarons, bipolarons, clusters, or fluctuations.[15,19]

Figure 2 is a plot of the data for sample $A1$. The curves through the data are from global least-square fits—see below. Samples A and $A2$ give similar results. There are four components of the low-temperature specific heat: a hyperfine term, $C_{\rm hyp}(H)$, which is responsible for the upturns in C/T vs T at the lower temperatures; an EDOS term, $C_{\rm EDOS}(H)$; an H-independent lattice term, $C_{\rm lat}$; and, expected based on the inelastic neutron-scattering data,[9–13] a ferromagnetic spin-wave term, $C_{\rm fsw}(H)$.

The hyperfine term, due to the Mn nuclei, is represented by the first term of the high-T expansion of a Schottky function,

$$C_{\rm hyp}(H)=A(H)/T^2=G[H_{\rm hyp}(H)/T]^2, \tag{1}$$

where $G=\Sigma f N_A g_N^2 I(I+1)\mu_N^2/3k_B=\Sigma f N_A[(I+1)/I]\times u_N^2\mu_N^2/3k_B$ with N_A being Avagadro's number, k_B the Boltzmann constant, f the fractional isotopic abundance, g_N the nuclear spectroscopic-splitting factor, I the nuclear spin, μ_N the nuclear magneton, and $u_N\equiv\mu/\mu_N=g_N I$. The EDOS term is given by

$$C_{\rm EDOS}(H)=\gamma(H)T, \tag{2}$$

where γ may be H dependent—see below. Representation of the lattice component is by the harmonic-lattice expansion

$$C_{\rm lat}=\sum B_n T^n, \tag{3}$$

where $n=3,5,7,\ldots$. The number of terms needed to represent $C_{\rm lat}$ is determined by the particular substance and fitting range. Only long-wavelength spin waves are excited at low temperatures, and hydrodynamic Heisenberg spin-wave theory, which is generally valid for both insulators and metals,[20,21] applies. In the temperature regime $T<12.5$ K, T is $<0.15T_C$ and the expression

$$C_{\rm fsw}(H)=B_{\rm fsw}T^{3/2}\int F(\Delta,g,H,T)dx \tag{4}$$

should apply,[22] where Δ is the anisotropy related spin-wave gap (zero for cubic symmetry) and g is the spectroscopic-splitting factor. $B_{\rm fsw}=[V(k_B/4\pi^2)(k_B/D)^{3/2}]$ where D is the spin-wave stiffness constant and V is the molar volume. The expression $\int F(\Delta,g,H,T)dx$ is given explicitly by

$$\int_{(\Delta+g\mu_B H)/k_B T}^{\infty}\{[x^2e^x/(e^x-1)^2]\times[x-(\Delta+g\mu_B H)/k_B T]^{1/2}\}dx, \tag{5}$$

where $x=[\Delta+g\mu_B H+Dk^2]/k_B T$ and μ_B is the Bohr magneton. For $H=0$ and $\Delta=0$ the integral of Eq. (5) has a value 4.458. For nonzero values of either H or Δ the integral must be evaluated numerically. The term $g\mu_B H$ corresponds to an additional gap in the spectrum when $H\neq 0$. For $H=0$ and $\Delta\neq 0$ $C_{\rm fsw}$ can be approximated[23] by

$$C_{\rm fsw}(0)=\Lambda_{\rm fsw}T^{3/2}e^{-\delta/T}, \tag{6}$$

where $\Lambda_{\rm fsw}\sim 4.5B_{\rm fsw}$ and $\delta\sim\Delta/2k_B$.

Several preliminary fits to the $H=0$ data were made to establish the reality of the spin-wave contribution and its form. Since the larger sample A has the highest precision specific heats, it was used at this stage of the analysis. The fitting expression used was of the form

$$C(0)=A(0)/T^2+\gamma T+\Lambda_{\rm fsw}T^m e^{-\delta/T}+\sum B_n T^n. \tag{7}$$

A series of fits, fixing $m=3/2$, were carried out over the intervals $1<T<4$ K and $1<T<12.5$ K. Within the rms deviations of the fits $\delta=0$, a result consistent with the inelastic neutron-scattering data that show no anisotropy gap. Several fits, with m as a variable and $\delta=0$, gave $m\sim 3/2$, which is consistent with the presence of ferromagnetic spin waves. For the smaller temperature interval, the rms deviation is not reduced by including a B_5T^5 lattice term; however, for the larger temperature interval such a term did reduce the rms deviation. As a further test of the assumption that a spin-wave term is present in the low-temperature data, Eq. (7) was modified by replacing $\Lambda_{\rm fsw}T^m e^{-\delta/T}$ with *two* additional lattice terms, B_7T^7 and B_9T^9, for the larger temperature interval. This *increased* the rms deviation of the fit from 0.095% to 0.25%, a result that supports the reality of a spin-wave term. We conclude that the appropriate fitting expression for $H=0$ is given by

$$C(0)=A(0)/T^2+\gamma T+4.458B_{\rm fsw}T^{3/2}+B_3T^3+B_5T^5. \tag{8}$$

TABLE I. Comparison of parameters derived from global least-square fits of the specific-heat data for $La_{0.65}Ca_{0.35}MnO_3$ [^{16}O and ^{18}O]. The fit range is 1–12.5 K. The measuring fields H (and the fields of the global fits) are given in the parentheses of the parameter list. Units are in ml, K, mole, and T unless otherwise specified. $\Theta_D=[12\pi^4RN_a/5B_3]^{1/3}$ is the Debye temperature where R is the gas constant and N_a the number of atoms per formula unit. D is the ferromagnetic spin-wave stiffness constant and Δ is the spin-wave energy gap. Numbers in parentheses following the parameter values are standard errors ($\pm$) and are to be associated with the least-significant digits.

Parameters	Sample $A1$ [^{16}O]	Sample $A1$ [^{16}O]	Sample $A2E$ [^{16}O]	Sample $1E$ [^{18}O]
A (0)	7.91(3)	7.53(5)	7.66(6)	7.92(7)
A (1)	8.18(4)	8.05(6)		
A (2)	7.66(4)	7.65(5)	7.52(7)	7.69(8)
A (3)	6.99(4)	7.03(5)		
A (5)	5.96(3)	5.92(5)	5.74(5)	6.13(7)
A (7)	5.13(3)	5.03(5)		
A (9)	4.38(2)	4.30(4)	4.29(4)	4.62(5)
γ (0) or γ	3.94(3)	4.29(1)	4.28(7)	4.15(8)
γ (1)	4.10(2)			
γ (2)	4.19(2)		4.56(5)	4.38(5)
γ (3)	4.25(2)			
γ (5)	4.27(1)		4.59(2)	4.48(2)
γ (7)	4.27(1)			
γ (9)	4.28(1)		$4.51(1_5)$	$4.47(1_5)$
B_{fsw}	0.183(7)	0.141(1)	0.166(8)	0.182(10)
D (meV Å^2)	141(6)	168(2)	151(8)	142(7)
Δ (K)	0 (fixed)	0 (fixed)	0 (fixed)	0 (fixed)
B_3	0.0757(8)	0.0827(5)	0.1280(21)	0.1190(23)
Θ_D (K)	505(2)	490(1)	424(2)	434(3)
B_5	$3.40(4)\times10^{-4}$	$3.09(4)\times10^{-4}$	$2.30(11)\times10^{-4}$	$2.75(11)\times10^{-4}$
rms deviation %	0.39	0.75	0.68	0.73

A global least-square fit was used to obtain the best values for the various parameters. Global least-square fits are better than single-field fits for determining parameters that are H independent because they tend to average out random systematic errors in the data that are related to those parameters, e.g., thermometer calibrations and addenda heat capacities. The fitting expression is

$$C(H)=A(H)/T^2+\gamma(H)T+B_{\mathrm{fsw}}T^{3/2}\int F(\Delta,g,H,T)dx + B_3T^3+B_5T_5, \quad (9)$$

where the integral in Eq. (9) was evaluated numerically for each value of H and T assuming an isotropic $g=2$ and $\Delta=0$. Several preliminary global fits were made before the final data analysis was done. Two global fits were made to the data of sample A using Eq. (9) and Eq. (9) with an additional B_7T^7 lattice term with no significant changes in either the rms deviations or the parameters. Parameters from these two global fits agreed with the corresponding ones from the single-field fits for $H=0$. A global fit with Δ/k_B fixed at 1 K produced only a small *increase* in the rms deviation and *small* changes in all of the parameters, confirming the conclusion of the single-field $H=0$ fit that $\Delta=0$. When a fitting range from 1 to 4 K is used, and the B_5T^5 term in Eq. (9) is dropped, the rms deviation decreases from 0.39 to 0.32% with only small changes, within their standard errors, to the parameters.

Inelastic neutron-scattering data found that the spin-wave stiffness constant D is temperature independent[11] in the range of the present fits. Fulde and Jensen[24] show that electronic masses are enhanced by interaction with spin waves and, since the spin waves are H dependent, this enhancement is also H dependent. The theory[24] accounts, semiquantitatively, for the decrease in $\gamma(H)$ found in the ferromagnetic Pr metal.[25] Global fits were made using either γT or $\gamma(H)T$ in Eq. (9). To evaluate the final parameters the temperature range for all global fitting is $1\leqslant T\leqslant 12.5$ K.

Table I summarizes the parameters derived from global least-square fits [using both γ and $\gamma(H)$ in Eq. (9)] to the specific-heat data for sample $A1$, which is representative of all the samples before the reprocessing. There is a strong co-dependency among the parameters except for $A(H)$, whose $A(H)T^2$ contribution to $C(H)$ is important only at the lower temperatures.

The curves in Fig. 2 represent the specific heats derived from the fits to the data of sample $A1$ using $\gamma(H)$ in Eq. (9). The deviations from the fits using γ in Eq. (9) are shown in Fig. 3(a) while those using $\gamma(H)$ are shown in Fig. 3(b). Use of the $\gamma(H)T$ term in place of γT in the fitting expression

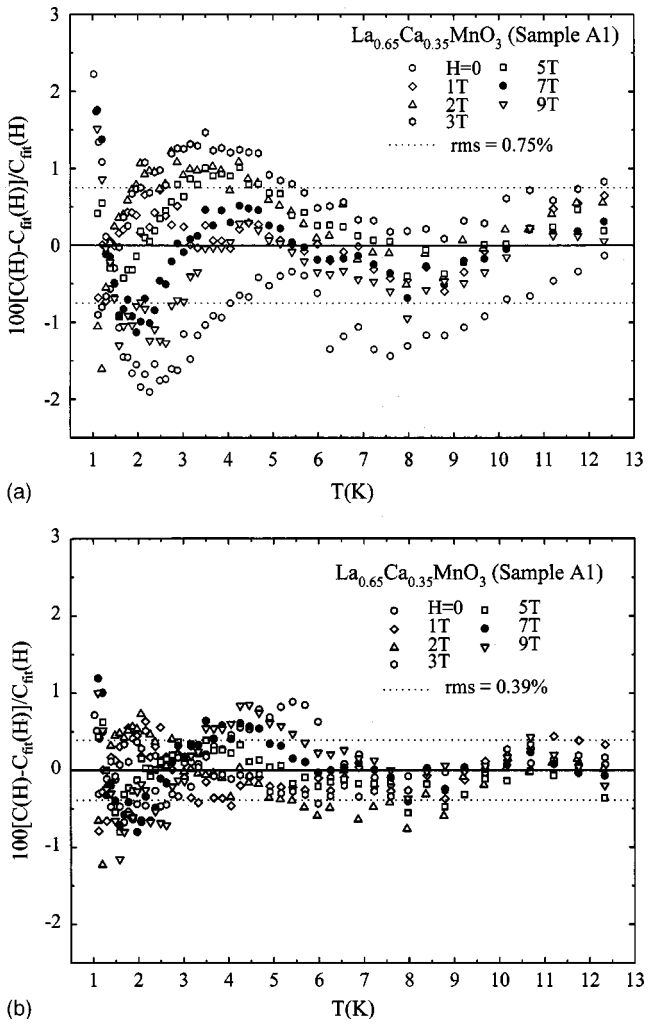

FIG. 3. (a) Deviations from a global least-square fit, with an H-independent γ, to the data shown in Fig. 2. The deviations do not have a uniform amplitude over the temperature range of the fit. In particular, they are larger below ~5 K. (b) Deviations from a global least-square fit, with an H-dependent γ, to the data shown in Fig. 2. In contrast to (a) the deviation amplitudes are more uniform and smaller.

reduces the rms deviation by a factor ~1.6 and essentially eliminates the ''lump'' of systematic deviations below ~5–6 K—see Figs. 3(a) and 3(b). The results for samples *A* and *A*2, not shown, are similar.

Figure 4 is a plot of the various specific-heat components for $H=0$ from the global fit to sample *A* using Eq. (9) with $\gamma(H)T$. At low temperatures, the $C_{\rm hyp}(0)$ term is dominant, while at high temperatures $C_{\rm lat}$ is the largest component. $C_{\rm fsw}(0)$ is smaller than $C_{\rm EDOS}(0)$ everywhere in the fitting range, although it must eventually cross over since it has a $T^{3/2}$ dependence vs the T dependence for $C_{\rm EDOS}(0)$. Also shown is $C_{\rm fsw}(9\ {\rm T})$ to illustrate the effect of H on the ferromagnetic spin-wave contribution. For $H=9$ T, the effect of the field-created gap in the spin-wave DOS is to produce a T dependence in $C_{\rm fsw}$ that is much stronger than $T^{3/2}$. Since increasing H lowers $C_{\rm fsw}(H)$ and raises $\gamma(H)$, the qualitative relationship between the two is valid for all fields of the present measurements.

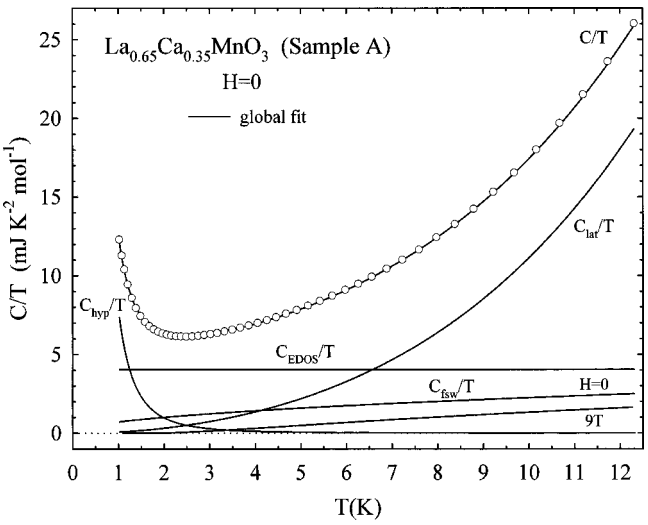

FIG. 4. C/T vs T plot of the contributions of the various components used in the global least-square fit of the specific-heat data for sample A. The components are shown for $H=0$ except for the ferromagnetic spin-wave contribution that is shown for both $H=0$ and 9 T.

B. Samples after ^{16}O/^{18}O exchange

Figure 5 is a plot of $C(0)/T$ vs T for samples *A*, *A*1*E*, and *A*2*E*. The specific heat of sample *A*2*E* is slightly greater at all temperatures than that of sample *A*1*E*, which is opposite to the expected isotope shift. More significantly, there is a very large increase in the specific heats for both of these samples compared to that of sample *A*.

Global least-square analysis was used to analyze the specific-heat data for samples *A*1*E* and *A*2*E* as described above in Sec. III A. As in the case of the parent samples, the fits using $\gamma(H)$ in Eq. (9) had significantly lower rms deviations, and a notably more uniform distribution of the devia-

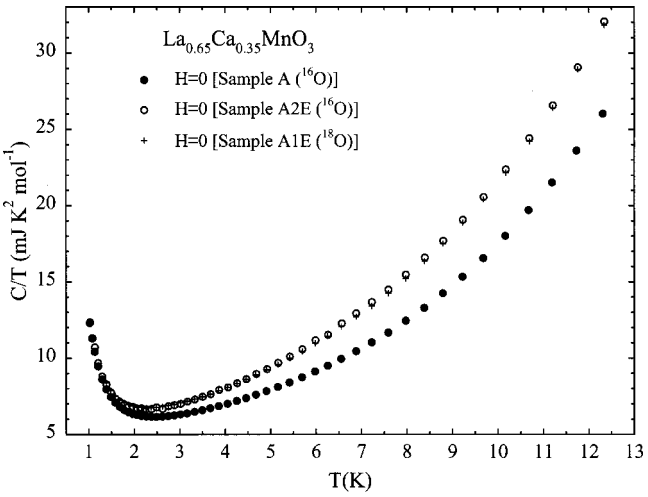

FIG. 5. $C(0)/T$ vs T for sample A and samples *A*1*E* and *A*2*E*, the parallel-processed ^{18}O and ^{16}O samples, showing the modification caused by the multiple processing cycles. For the two multiply processed samples, the specific heat for the ^{18}O sample lies lower than that for the ^{16}O sample. This decrease is *opposite* to that expected for the substitution of ^{18}O for ^{16}O.

tions from the fit, than those with an H-independent γ. In both instances, however, the rms deviations were larger than those of samples A, $A1$, and $A2$ reflecting, undoubtedly, the smaller sample sizes. The parameters are listed in Table I for the fits using $\gamma(H)$. Contributions from $C_{\rm hyp}(H)$ and $C_{\rm fsw}(H)$ are the same for all five samples—A, $A1$, $A2$, $A1E$, and $A2E$—to within a scatter (approximately equal to the standard errors) of $\pm 3\%$ and $\pm 4\%$, respectively. Sample $A2E$ had $\gamma(H)$'s that were systematically larger ($\sim 4\%$) than those of sample $A1E$. Both samples $A1E$ and $A2E$ had $\gamma(H)$'s that were systematically larger than those of the original ^{16}O samples by $\sim 5\%$ and $\sim 9\%$, respectively. Similarly, the $C_{\rm lat}$ contributions for the two parallel-processed samples were only slightly different, with B_3 for sample $A2E$ greater by $\sim 8\%$ than sample $A1E$, but with each having very much greater contributions (~ 50 and $\sim 60\%$ in B_3, respectively) than those of the original ^{16}O samples.

IV. DISCUSSION

A. The $C_{\rm EDOS}(H)$ component

The global least-square fits using a $\gamma(H)T$ term have a substantially smaller rms deviation than those using γT—see Table I. It could be argued that the increased number of parameters might account for the reduced rms deviation. However, in addition to the reduction, the deviations from the Eq. (9) fitting expression using $\gamma(H)$ have amplitudes that are essentially temperature independent, with no large systematic errors at the lower temperatures. This is in contrast to the case when an H-independent γ is used in Eq. (9)—see Figs. 3(a) and 3(b). It is these two results, together with the expectation of an interaction between the conduction electrons and the field-dependent ferromagnetic spin waves,[24] which lead to the selection of Eq. (9) with a $\gamma(H)T$ term as the best choice for the representation of the specific-heat data.

Figure 6 is a plot of $\gamma(H)$ vs H for all five samples that shows a systematic change with field. The variation of $\gamma(H)$ with H is qualitatively similar for all samples. At low fields $\gamma(H)$ increases and reaches a plateau at intermediate fields, with perhaps a *small* decrease at the highest field. [The small decrease in $\gamma(H)$ at 9 T is evident for sample A since it was larger and has a higher precision for the fitted parameters.] The scatter in the $\gamma(H)$'s from smooth curves through them is about equal to their standard errors—see Table I. A maximum in $\gamma(H)$ vs H is not predicted by the theory of Ref. 24, although it is similar to the results reported in Ref. 25. As shown in Fig. 4, $C_{\rm fsw}$ and $C_{\rm EDOS}$ are of comparable size and similar temperature dependence and, therefore, the apparent small maximum in $\gamma(H)$ might result from an error in the representation of $C_{\rm fsw}$. For example, by the assumption that $\Delta = 0$. However, fitting the data with $\Delta/k_B = 1$ K, rather than 0, did not change the rms deviation or any parameter values significantly, nor the H dependence of $\gamma(H)$.

Band-structure calculations[26–28] have been made for $La_{0.67}Ca_{0.33}MnO_3$ using both a ferromagnetic cubic perovskite and a ferromagnetic *Pnma* structure[29,30] that was refined by neutron measurements.[31] It was established that

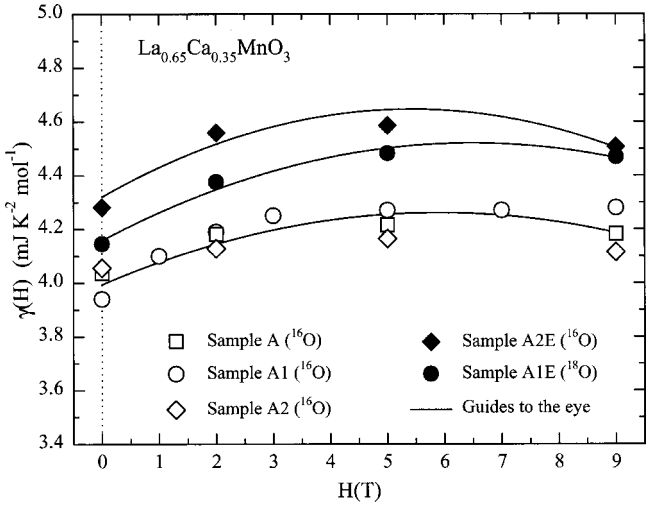

FIG. 6. $\gamma(H)$ vs H for the different $La_{0.65}Ca_{0.35}MnO_3$ samples. The variation of γ with H is theoretically predicted, and results from the interaction between the EDOS and the ferromagnetic spin waves. The two parallel-processed samples have $\gamma(H)$'s *larger* than the parent samples, and with $\gamma(H)$ for the ^{16}O sample *greater* than that of the ^{18}O sample.

$La_{0.67}Ca_{0.33}MnO_3$ is half metallic at low temperature, which means that the conduction is limited to a single Mn up-spin channel of majority carriers.[27] The Mn down-spin channels are localized;[27] consequently, the normal emission and adsorption of spin waves at finite temperatures are forbidden since there are no conducting states at low energy to scatter into by spin flip. Low-temperature spin-wave scattering for the up-spin channel is due primarily to phonons, or to spin-conserving electron-electron processes.[27] In Ref. 28 $N_{b\uparrow}(E_F)$, the band-structure EDOS for the majority up-spin conduction channel for $La_{0.67}Ca_{0.33}MnO_3$ with the ferromagnetic *Pnma* structure, was found to be 0.68 eV^{-1} for $H = 0$. The Sommerfeld constant, measured in units of mJ K^{-2} mol^{-1}, is given by $\gamma = 4.72N_{\uparrow}(E_F) = 4.72(1+\lambda)N_{b\uparrow}(E_F) = 3.2(1+\lambda)$, where λ is an interaction parameter arising from electron-phonon, electron-electron, and possible electron-magnon interactions. Samples A, A_1, and A_2 had an average value for $\gamma(0)$ of 4.0 mJ K^{-2} mol^{-1}. Thus, $\lambda = 0.25$ and, from $m^*/m_b = (1+\lambda)$, $m^* = 1.25m_b$ where m^* and m_b are the zero-field electron and band-structure electron masses, respectively.

Samples $A1E$ and $A2E$ have derived values of $\gamma(H)$ that are larger than those of the original ^{16}O samples, and which also differ slightly from one another—see Fig. 6 and Table I. These differences in $\gamma(H)$ probably reflect a superposition of effects caused by both the ^{18}O isotope substitution for ^{16}O and by the many parallel-processing cycles that were necessary to achieve ^{18}O homogeneity. For sample $A1E$[^{18}O] $\lambda = 0.30$ ($m^*/m_b = 1.30$), and for sample $A2E$[^{16}O] $\lambda = 0.34$ ($m^*/m_b = 1.34$). These differences in λ are nearly within the standard errors and may not be significant; however, Kresin[32] has recently predicted that substitution of ^{18}O for ^{16}O in the manganites will cause a *decrease* in $\gamma(H)$ of about the magnitude observed—see Table I.

B. The $C_{\rm fsw}(H)$ component

The spin-wave stiffness constant D for the various global fits using Eq. (9) with γ are 169(2), 168(2), and 166(2) meV Å^2, respectively, for samples A, $A1$, and $A2$. Equation (9) with $\gamma(H)$ gives $D=155(6)$ meV Å^2 for sample A, which is also the value obtained from inelastic-neutron scattering,[11] while samples $A1$ and $A2$ have D's of 141(6) and 160(8) meV Å^2, respectively. A global fit for sample $A1$ with D fixed at 155 meV Å^2 produces no change in the rms deviation, and only small changes in the other parameters. An average value of the stiffness constant for the five samples, using $\gamma(H)$ in Eq. (9), is $\langle D\rangle=150(9)$ meV Å^2, where the uncertainity is essentially equal to the standard errors. Using this $\langle D\rangle$ fixed in global fits of the five samples has a negligible effect on their rms deviations or the values of their parameters. Because the stiffness constant D is proportional to T_C, and since $T_C(^{18}\mathrm{O})/T_C(^{16}\mathrm{O})=0.97$ for $H=0$, there should be a corresponding shift in D. For samples $A1E$ and $A2E$, $D(^{18}\mathrm{O})/D(^{16}\mathrm{O})=142(7)/151(8)=0.94(5)$, which is comparable to the T_C ratio, but is also well within the standard errors of the D's. Because of the strong codependency of the various parameters, the agreement is probably accidental, especially since the spread in the fitted values of D for samples A, $A1$, and $A2$ is 19 meV Å^2.

Evidently, the additional processing cycles of samples $A1E$ and $A2E$, and the exchange of ^{18}O for ^{16}O, has no significant, or very large, effect on $C_{\rm fsw}(H)$. The good agreement of D obtained from inelastic-neutron scattering[11] with that derived from global least-square fits to the specific-heat data for all five samples provides further evidence of the accuracy of the data and the validity of Eq. (9) with $\gamma(H)$ as the proper fitting expression to use in the analysis.

C. The $C_{\rm hyp}(H)$ component

The $A(H)$ parameters, derived from the global fits of the specific-heat data, provide information about the hyperfine magnetic field at the ^{55}Mn nuclei. ^{55}Mn is the only naturally occurring isotope ($f=1$) with a spin $I=5/2$ and $u_N=3.461$, which gives $G=6.221\times10^{-3}$ mJ K T^{-2} mol^{-1}. It follows from Eq. (1) that

$$H_{\rm hyp}(H)=[A(H)/G]^{1/2}. \tag{10}$$

Figure 7 is a plot of $A(H)$ vs H for all five samples. There does not appear to be any systematic deviations among the five data sets, which have a maximum spread of ~3% for a given H, with a maximum deviation from the curve through them of ~3%. This provides proof that whatever the cause of the drastic changes in the specific heats of samples $A1E$ and $A2E$ it had little or no effect on $C_{\rm hyp}(H)$.

Using Eq. (10) allows $H_{\rm hyp}(H)$ to be calculated, and the results are plotted in Fig. 8 as a function of $H_{\rm int}$, the internal magnetic field. $H_{\rm int}$ is given by

$$H_{\rm int}=H-aM/V, \tag{11}$$

where α is the demagnetizing factor, M the magnetic moment, and V the molar volume. For $H>0.5$ T, in the range 1–12.5 K, M is essentially constant at the saturation value,

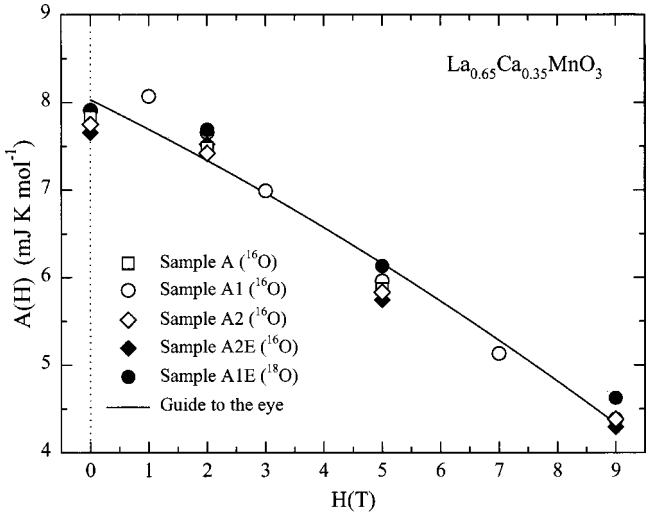

FIG. 7. $A(H)$ vs H demonstrating that the applied magnetic field is in opposition to the hyperfine magnetic field at the Mn nuclei.

$M_{\rm sat}=3.65N_A\mu_B=20.4$ kG cm^3 mol^{-1} (in Gaussian units), which produces a constant demagnetizing field. Approximating α by the value for a sphere, the correction gives $H_{\rm int}=H-0.25$ T. As H *increases* $H_{\rm hyp}(H)$ *decreases* indicating an *antiparallel* alignment of the intrinsic Mn hyperfine field $H_{\rm hyp}(0)$ with respect to the fields H and $H_{\rm int}$. The straight line is a least-squares fit of the data to the equation

$$H_{\rm hyp}(H)=H_{\rm hyp}(0)+\beta H_{\rm int}. \tag{12}$$

where $H_{\rm hyp}(0)=36.1(2)$ T and $\beta=-1.1(1)$.

Nuclear-magnetic-resonance (NMR) measurements are reported for $La_{0.67}Ca_{0.33}MnO_3$ in fields to 6 T.[33] The source of $H_{\rm hyp}(0)$ is primarily from core polarization by the Mn magnetic moments, with contributions from other sources being negligibly small.[33] Only a single narrow resonance line

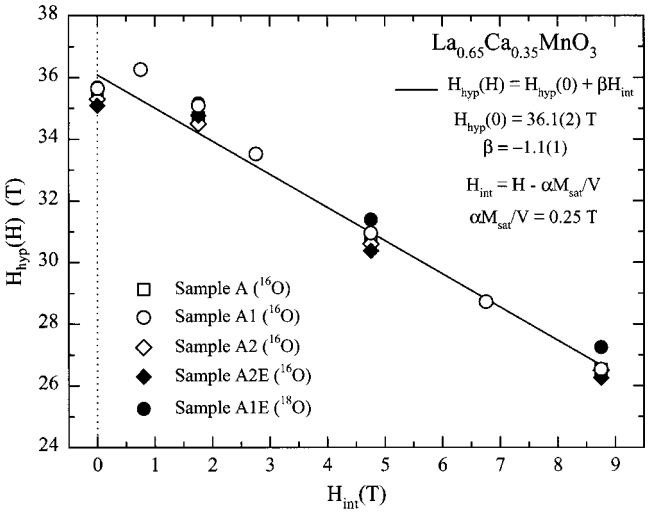

FIG. 8. $H_{\rm hyp}(H)$ vs $H_{\rm int}$ where $H_{\rm int}$ is the internal magnetic field resulting from the application of a demagnetization correction to the applied field. The straight line represents a least-squares fit to all the data, and demonstrates that H and $H_{\rm int}$ are antiparallel to $H_{\rm hyp}(0)$, the field at the Mn nuclei resulting from core polarization.

is observed at temperatures in the range 4.2 to 250 K. $H_{\rm hyp}(0)$ is 36.3 T at low temperatures, which is in very good agreement with the value derived from the specific-heat data, 36.1(2) T. In applied fields the spin-echo resonance lines[33] are shifted towards lower frequencies with a slope of $\beta=-1.4$ indicating an antiparallel orientation of the Mn hyperfine field with H. The value $\beta=-1.4$ is in reasonable agreement with $\beta=-1.1$ derived from the specific-heat data. The nearly congruent $H_{\rm hyp}(0)$'s and the similar shift in $H_{\rm hyp}(H)$ with H, is additional evidence that the specific-heat data are accurate, and that the Eq. (9) fitting expression with $\gamma(H)$ is valid.

The single narrow resonance line observed in the NMR measurements[33] can be satisfactorily explained if the hopping time τ_h of the carriers in the double-exchange coupling is much shorter than the period of the Larmor precession, τ_L, of the Mn nuclear spins. (If $\tau_h > \tau_L$, a broadened or double-resonance peak would be expected because of the different environments for Mn^{3+} and Mn^{4+}.) When $\tau_h \ll \tau_L$ the Mn nuclei are subject to an averaged hyperfine field, corresponding to an average Mn^{3+}/Mn^{4+} state, and a resulting single-resonance peak. There is, however, another possibility. Zero-field NMR signals[33] have been detected well above T_C, which are interpreted as providing direct evidence for the presence of magnetic polarons. A recent theory[19] of magnetic polarons/bipolarons describes the polaron as consisting of two adjacent Mn^{3+} ions bound by a p hole $(+)$ in the oxygen band, with the net spin of the two Mn^{3+} ions antiparallel to that of the p hole. The polarons are dynamic and move throughout the lattice involving all of the Mn^{3+} ions. In this theory all Mn have the same valence and surroundings and, therefore, a single NMR resonance line.

D. The $C_{\rm lat}$ component

The harmonic-lattice coefficients B_3 and B_5 from the global fits are listed in Table I. Also listed are the Debye temperatures Θ_D calculated using

$$\Theta_D=[(12/5)\pi^4 R N_a/B_3]^{1/3}, \tag{13}$$

where R is the gas constant and N_a the number of atoms in a formula unit. Figure 9 is a plot of $C_{\rm lat}/T^3$ vs T, where $C_{\rm lat}$ was calculated using B_3 and B_5 obtained from the various fits. Within the statistical uncertainty of the fits, samples A, $A1$, and $A2$ have the same specific heat. On the other hand, $C_{\rm lat}$—and the total $C(H)$—for samples $A1E$ and $A2E$ are drastically increased (a softening of the lattice modes). These large changes in $C_{\rm lat}$ for the O-exchanged samples are probably related to the additional processing, which could result in altering of the microstructure that is related to the separation into ferromagnetic insulating and percolation-connected conducting phases[34] below T_C. The T^3 lattice component is affected more than the T^5 component and in the opposite direction. At 1 K there is a ~50% increase in $C_{\rm lat}$ compared to a ~23% increase at 12.5 K. The B_3 parameter is *increased* by ~50% while B_5 is *decreased* by ~12%. This implies that it is the long-wavelength acoustic phonon modes that changed the most as a consequence of the multiple processing cycles.

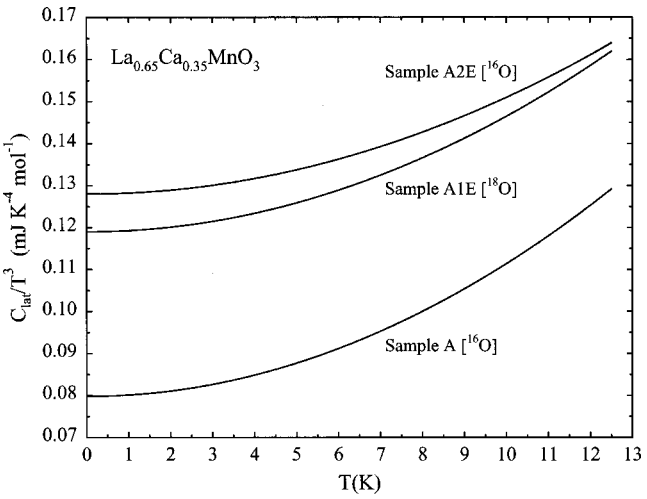

FIG. 9. $C_{\rm lat}/T^3$ vs T showing the shift of the lattice specific heat due to the multiple parallel-processing cycles used in the $^{16}O/^{18}O$ exchange. The low-temperature *decrease* in the lattice specific heat for the ^{18}O sample, compared with that for the reference ^{16}O sample, is *opposite* to that expected for the isotopic oxygen substitution.

$C_{\rm lat}$ and $C(H)$ for samples $A1E$ and $A2E$ also differ. The difference in $C_{\rm lat}$ for the two samples is in the *opposite* direction of that expected for the isotope effect resulting from the $^{18}O/^{16}O$ exchange. At low temperatures, in the T^3 region, $C_{\rm lat}$ is related approximately[35] to the masses (m_a) making up the sample by the proportionality

$$C_{\rm lat} \propto \sum (m_a)^{3/2} \propto ({\rm MW})^{3/2}. \tag{14}$$

For samples $A1E$ and $A2E$, the ratio $C_{\rm lat}[^{18}O]/C_{\rm lat}[^{16}O] = (212.35/207.25)^{3/2} = 1.037$, an expected ~4% *increase* in $C_{\rm lat}$ for the ^{18}O material, as opposed to the observed *decrease* in the $C_{\rm lat}$ ratio. This ratio varies monotonically from 7% at 1 K to 1.2% at 12.5 K where dispersion, measured by the T^5 term, is becoming increasingly important. Apparently, those modifications resulting from the multiple processing cycles have masked the isotope shift in $C_{\rm lat}$ at low temperatures, although it appears to be present in the high-temperature specific-heat data.[15]

V. SUMMARY

The specific heat of a near-optimally doped polycrystalline sample of $La_{0.65}Ca_{0.35}MnO_3$, with $T_C = 265$ K, was measured in the temperature range $1 \leqslant T \leqslant 32$ K for $0 \leqslant H \leqslant 9$ T. An excellent global least-square fit to the data is obtained using four components: hyperfine, EDOS, ferromagnetic spin wave, and lattice terms in the fitting expression. Both the hyperfine and spin-wave contributions are in quantitative agreement with NMR (Ref. 33) and inelastic-neutron-scattering results,[11] respectively. This agreement supports the validity of both the data and their analysis. For $H=0$ there is an enhancement of the band-structure EDOS (Ref. 28) by a factor of 1.25. The EDOS contribution is magnetic-field dependent, which is predicted theoretically[24]

because of electron-magnon coupling.

Specific heat was measured for two pieces cut from the original ^{16}O parent sample after multiple parallel-processing steps to produce matching ^{18}O and ^{16}O samples. Ferromagnetic spin-wave and hyperfine parameters are the same for the parent sample and these two samples to within their standard errors. The lattice specific heat of the ^{16}O reference sample was a little larger than the ^{18}O sample, which is *not* in accord with the anticipated isotope-effect shift. EDOS contributions also differ by small amounts, with that of the ^{16}O sample being greater. The enhancements of the band-structure density of states for $H=0$ are 1.34 and 1.30 for the ^{16}O and ^{18}O samples, respectively. Both of the parallel-processed samples have very much larger lattice contributions ($\sim$50% greater at low temperatures), and—to a lesser extent—larger EDOS components ($\sim$10% greater) than the parent sample. Evidently, the many processing cycles necessary to produce ^{18}O homogeneity are responsible for these modifications, probably related to variable microstructures.[34] This extreme sensitivity to processing serves as a warning of the inherent hazards associated with the comparison of parameters obtained from different samples.

ACKNOWLEDGMENTS

The work at Lawrence Berkeley National Laboratory was supported by the Director, Office of Basic Energy Sciences, Materials Sciences Division of the U.S. Department of Energy under Contract No. DE-AC03-76SF00098. The work at the University of Alberta was supported by grants from the Natural Sciences and Engineering Research Council of Canada. The work at Amherst was supported by an Amherst College Faculty Research Grant.

[1] J. M. D. Coey, M. Viret, L. Ranno, and K. Ouanadjela, Phys. Rev. Lett. **75**, 3910 (1995).
[2] S. N. Bai, Y. Y. Chen, Y. D. Yao, L. H. Chen, S. H. Lin, and Y. Liou, Chin. J. Phys. (Taipei) **34**, 798 (1996).
[3] J. J. Hamilton, E. L. Keatley, H. L. Ju, A. K. Raychaudhuri, V. N. Smolyaninova, and R. L. Greene, Phys. Rev. B **54**, 14 926 (1996).
[4] L. Ghivelder, I. Abrego Castillo, N. McN. Alford, G. J. Tomka, P. C. Riedi, J. MacManus-Driscoll, A. K. M. Akther Hossain, and L. F. Cohen, J. Magn. Magn. Mater. **189**, 274 (1998).
[5] T. Okuda, Y. Tomioka, A. Asamitsu, and Y. Tokura, Phys. Rev. B **61**, 8009 (2000).
[6] M. Roy, J. F. Mitchell, S. J. Potashnik, and P. Schiffer, J. Magn. Magn. Mater. **218**, 191 (2000).
[7] B. F. Woodfield, M. L. Wilson, and J. M. Byers, Phys. Rev. Lett. **78**, 3201 (1997).
[8] T. Okuda, A. Asamitsu, Y. Tomioka, T. Kimura, Y. Taguchi, and Y. Tokura, Phys. Rev. Lett. **81**, 3203 (1998).
[9] J. W. Lynn, R. W. Erwin, J. A. Borchers, Q. Huang, A. Santoro, J.-L. Peng, and Z. Y. Li, Phys. Rev. Lett. **76**, 4046 (1996).
[10] L. Vasiliu-Doloc, J. W. Lynn, A. H. Moudden, A. M. de Leon-Guevara, and A. Revcolevschi, J. Appl. Phys. **81**, 5491 (1997).
[11] J. W. Lynn, R. W. Erwin, J. A. Borchers, A. Santoro, Q. Huang, J.-L. Peng, and R. L. Greene, J. Appl. Phys. **81**, 5488 (1997).
[12] Y. Endoh and K. Hirota, J. Phys. Soc. Jpn. **66**, 2264 (1997).
[13] J. A. Fernandez-Baca, P. Dai, H. Y. Hwang, C. Kloc, and S.-W. Cheong, Phys. Rev. Lett. **80**, 4012 (1998).
[14] Heilman *et al.*, Phys. Rev. B **61**, 8950 (2000).
[15] J. E. Gordon, C. Marcenat, J. P. Franck, I. Isaac, Guanwen Zhang, R. Lortz, C. Meingast, F. Bouquet, R. A. Fisher, and N. E. Phillips (unpublished).
[16] J. P. Franck, in *Physical Properties of High Temperature Superconductors IV*, edited by D. M. Ginsberg (World Scientific, Singapore, 1994), p. 189.
[17] J. E. Gordon, R. A. Fisher, Y. X. Jia, N. E. Phillips, S. F. Reklis, D. A. Wright, and A. Zettl, J. Magn. Magn. Mater. **177–181**, 856 (1998); Phys. Rev. B **59**, 127 (1999).
[18] R. A. Robie and B. S. Hemingway, J. Chem. Thermodyn. **17**, 165 (1985).
[19] A. S. Alexandrov and A. M. Bratkovsky, J. Phys.: Condens. Matter **11**, 1989 (1999).
[20] B. I. Halperin and P. C. Hohenberg, Phys. Rev. **177**, 952 (1969).
[21] J. W. Lynn (private communication).
[22] C. Kittel, *Quantum Theory of Solids* (Wiley, New York, 1963), p. 49.
[23] K. Niira, Phys. Rev. **117**, 129 (1960).
[24] P. Fulde and J. Jensen, Phys. Rev. B **27**, 4085 (1983); P. Fulde (private communication).
[25] E. M. Forgan, Physica B **107**, 65 (1981).
[26] W. E. Pickett and D. J. Singh, Phys. Rev. B **53**, 1146 (1996).
[27] W. E. Pickett and D. J. Singh, Phys. Rev. B **55**, R8642 (1997).
[28] D. J. Singh and W. E. Pickett, Phys. Rev. B **57**, 88 (1998).
[29] E. O. Wollan and W. C. Koehler, Phys. Rev. **100**, 545 (1955); J. B. A. A. Elemans, B. van Laar, K. R. van der Veen, and B. O. Loopstra, J. Solid State Chem. **3**, 238 (1971).
[30] Q. Huang, A. Santoro, J. W. Lynn, R. W. Erwin, J. A. Borchers, J.-L. Peng, and R. L. Greene, Phys. Rev. B **55**, 14 987 (1997).
[31] P. Dai, J. Zhang, H. A. Mook, S. H. Liou, P. A. Dowben, and E. W. Plummer, Phys. Rev. B **54**, R3694 (1996).
[32] V. Z. Kresin (private communication).
[33] Cz. Kapusta, P. C. Riedi, G. J. Tomka, W. Kocemba, M. R. Ibarra, J. M. De Teresa, M. Viret, and J. M. D. Coey, J. Phys.: Condens. Matter **11**, 4079 (1999); Cz. Kapusta, P. C. Riedi, W. Kocemba, M. R. Ibarra, and J. M. D. Coey, J. Appl. Phys. **87**, 7121 (2000).
[34] See, e.g., M. O. Dzero, L. P. Gor'kov, and V. Z. Kresin, Eur. Phys. J.: Appl. Phys. **14**, 459 (2000); A. Moreo, S. Yunoki, and E. Dagotto, Science **283**, 2034 (2000); R. H. Heffner, J. E. Sonier, D. E. McLaughlin, G. J. Nieuwenhuys, G. Ehlers, F. Mezei, S.-W. Cheong, J. S. Gardner, and H. Röder, Phys. Rev. Lett. **85**, 3285 (2000); J. M. Zuo and J. Tao, cond-mat/0009472 (unpublished).
[35] F. A. Lindemann, Phys. Z. **11**, 609 (1910).